



## Letter

**Cite this article:** Huidobro J, Aramendia J, Arana G, Hausrath EM, Madariaga JM (2023). The effect of low temperature on the Raman spectra of calcium-rich sulfates on Mars. *Annals of Glaciology* 1–6. <https://doi.org/10.1017/aog.2023.29>

Received: 24 October 2022

Revised: 26 March 2023

Accepted: 28 March 2023

**Keywords:**



Applied glaciology; frozen ground; ice temperature; remote sensing

**Corresponding author:**

Jennifer Huidobro;

E-mail: [jennifer.huidobro@ehu.es](mailto:jennifer.huidobro@ehu.es)

# The effect of low temperature on the Raman spectra of calcium-rich sulfates on Mars

Jennifer Huidobro<sup>1</sup> , Julene Aramendia<sup>1</sup>, Gorka Arana<sup>1</sup>, Elisabeth M. Hausrath<sup>2</sup> and Juan Manuel Madariaga<sup>1</sup> 

<sup>1</sup>Department of Analytical Chemistry, University of the Basque Country (UPV/EHU), Barrio Sarriena s/n, Leioa 48940, Spain and <sup>2</sup>Department of Geoscience, University of Nevada, Las Vegas (UNLV), 4505 S. Maryland Parkway, Las Vegas, NV 89154-4010, USA

**Abstract**

Raman spectra (532 nm diode laser) of gypsum, syngenite and görgeyite powders were studied from 273 to 83 K every –10 K. Although it was found that not all the Raman peaks are temperature-sensitive, the effect of temperature on the Raman signal of some bands was modelled. It was observed that the main bands of the three sulfates shift toward higher wavenumbers as temperature decreases. The strengthening of the bonds causes an increase in energy and, consequently, higher wavenumbers. However, –OH bands shift depending on the crystal structure they acquire as the temperature decreases, so not all –OH bands behave in the same way. Finally, the gypsum –OH bands change to more ordered crystalline structures with decreasing temperature, so their bandwidths become narrower and sharper.

**1. Introduction**

Research done by rovers, orbiters and landers revealed that a substantial portion of the existing water on Mars today is in the form of ice. In addition, a tiny amount of water is present as water-vapor in the atmosphere and low-volume liquid brine can be found in shallow soil areas (Nazari-Sharabian and others, 2020).

Apart from the main areas where water is located (solid, liquid and vapor), Mars has a fraction of its water in the structures of plentiful water-rich materials, such as in sulfates and clay minerals (phyllosilicates) (Nazari-Sharabian and others, 2020). This fact is well known because the spectro-imaging instrument (OMEGA) on the Mars Express provided the first detection of hydrated compounds on Mars (Gendrin and others, 2005).

Chemical interactions between water, atmospheric gases and radiation with rocks weather nominally anhydrous materials formed by volcanic and igneous processes (primary minerals) into hydrous phases (secondary minerals), including clay minerals. During the process, some of them combine water (OH<sup>–</sup> or H<sub>2</sub>O) into their crystalline structures, forming hydrated minerals (Ehlmann and others, 2011; Nazari-Sharabian and others, 2020).

In fact, the OMEGA and CRISM visible/near-infrared orbital imaging spectrometers, on board the Mars Express and Mars Reconnaissance Orbiter spacecraft, respectively, revealed many hotspots where hydrated minerals are present on Mars. Thanks to these results, it has been possible to create maps to visualize these hot spots (Ehlmann and others, 2011; Carter and others, 2013).

Some of the minerals detected by both instruments were kieserite (MgSO<sub>4</sub>·H<sub>2</sub>O), an unspecified hydrated sulfate, gypsum [CaSO<sub>4</sub>·2H<sub>2</sub>O] (Huidobro and others, 2022*bb*), phyllosilicates (kaolinite [Al<sub>2</sub>Si<sub>2</sub>O<sub>5</sub>(OH)<sub>4</sub>] (Brindley and Robinson, 1946) and montmorillonite [(Ca, Na)<sub>0.16</sub>(Al,Mg,Fe)<sub>2.08</sub>(Si,Al)<sub>4</sub>O<sub>10</sub>(OH)<sub>2</sub>·nH<sub>2</sub>O]) (Uddin, 2008), among others (Cloutis and others, 2007; Nazari-Sharabian and others, 2020). Previously, it was already indicated that the unknown sulfate found by OMEGA and CRISM is magnesium and calcium-rich (Chou and Seal, 2007), so it is possible that this sulfate could be syngenite [K<sub>2</sub>Ca(SO<sub>4</sub>)<sub>2</sub>·H<sub>2</sub>O] and/or görgeyite [K<sub>2</sub>Ca<sub>5</sub>(SO<sub>4</sub>)<sub>6</sub>·H<sub>2</sub>O] (García-Florentino and others, 2021).

Today, many studies are being carried out in cold terrestrial areas, such as the poles, to locate aqueous sulfate sources that can provide insight into the surface hydrological conditions and sulfur cycle on Mars (Szynkiewicz and Bishop, 2021). In addition, many meteorites from Mars are found in environments that are sometimes also cold, such as the deserts of Africa or Antarctica, and hydrated sulfates have been found in Antarctica Martian meteorites. This suggests that the contribution of hydrated sulfates in the meteorites may be due to two possible processes. The first consists of the terrestrial weathering of the sample, through which the sulfates come from the Earth and enter into the meteorite by alteration processes (Huidobro and others, 2022*bb*). The second possibility is that these sulfates are secondary minerals from Mars, remaining in the sample since its ejection. In this case, meteorites can be considered the key to obtain clues about the primary geologic processes in Mars and to identify its ancient sulfur cycle (Nazari-Sharabian and others, 2020).

In this sense, the study of hydrated sulfates in polar environments, both on Earth and on Mars, is very important to recreate the planet's water history. In fact, two missions were sent to the Martian poles, the Mars Polar Lander that was lost at its arrival in 1999, and the Phoenix Mars mission, which launched the Phoenix lander to the north Martian pole and indeed

© The Author(s), 2023. Published by Cambridge University Press on behalf of The International Glaciological Society. This is an Open Access article, distributed under the terms of the Creative Commons Attribution licence (<http://creativecommons.org/licenses/by/4.0/>), which permits unrestricted re-use, distribution and reproduction, provided the original article is properly cited.

[cambridge.org/aog](http://cambridge.org/aog)

detected water ice in 2008. In the near future, it is possible that more missions will be sent to the poles of Mars, to study water ice and hydrated minerals. Vibrational spectroscopies are very useful techniques for the study of hydrated minerals due to its high sensitivity to structural variations caused by differences in physical magnitudes, such as temperature. Therefore, Raman spectroscopy is a vibrational technique that is gradually gaining importance in space missions. In fact, it is possible that the next robotic mission to the Martian poles could be equipped with a Raman spectrometer to analyze the permafrost and the hydrated minerals that are expected to be found. In fact, Raman spectroscopy has already traveled to Mars on board the Perseverance rover. Moreover, it will travel on board the MMX mission and the ExoMars mission in a few years (Huidobro and others, 2022a).

In addition, Raman spectroscopy could be used to determine the temperature of a material because temperature can affect the peak position of some Raman bands. When a Raman band shifts significantly with temperature, the monitoring of the band position is the most straightforward methodology of determining temperature (Tuschel, 2016). In contrast, if the temperature of the sample is known, using the relationship between Raman signal of the bands that shift it and the temperature it is possible to estimate at what wavenumber the Raman peaks may appear.

At least, two distinct effects of a change in scattering could occur with temperature changes. Firstly, the temperature change could cause a change in the molecular structure of the compound, such as association of simple molecules into more complex aggregates, or a change in the crystalline form of the substance. Secondly, a change in temperature could produce a new distribution of the molecules in the various rotational and vibrational energy levels (Sutherland, 1933). What is clear is that a change in temperature would result in band alteration or in the appearance of new bands, an effect that can be monitored by Raman spectroscopy.

Therefore, the aim of this work is to estimate the relation between the Raman signal and the temperature for the sulfates gypsum, syngenite and görgeyite at low temperatures. The estimation will be based on the monitoring of the Raman shift that the temperature-sensitive bands undergo with decreasing temperature between 273 and 83 K. Although no temperature has ever been recorded on Mars below 133 K (NASA, 2023), calibrates were performed from 273 to 83 K in order to make the linear estimates more robust.

Even though studies of the influence of temperature or pressure on the Raman spectra of gypsum have been made previously (Couty and others, 1983; Schofield and others, 2000; Chio and others, 2004; Weber and others, 2018; Madariaga and others, 2020), this work analyzes for the first time this dependence for syngenite and görgeyite, two hydrated sulfates expected to be found on Mars, under low temperatures.

## 2. Samples

Previously synthesized gypsum, syngenite and görgeyite powders were used as reagents for this work (García-Florentino and others, 2021).

## 3. Instrumentation and methodology

### 3.1. Instrumentation

#### *MicroRaman spectroscopy*

This work was performed using the Renishaw InVia confocal microRaman spectrometer (Renishaw, UK). The instrument is equipped with 785 and 532 nm excitation diode lasers

(Renishaw UK RL785 with a nominal 45 mW output power and Renishaw UK RL532C50 with a nominal 300 mW output power, respectively) and with a CCD detector cooled by the Peltier effect. In addition, the instrument is coupled to a Leica DMLM microscope (Bradford, UK), implementing an XYZ Stage Control toolbar and equipped with a micro camera for searching the points of interest. 5× N PLAN (0.12 NA) and 20× N PLAN EPI (0.40 NA) lenses and 50× N PLAN (0.75 NA) long-range objectives were used for visualization and focusing. The nominal power of the source can be modulated between 0.0001 and 100% of the total power to avoid thermo-decomposition of the sample. The InVia spectrometer is daily calibrated setting the 520.5 cm<sup>-1</sup> silicon line and has a ±1 cm<sup>-1</sup> of spectral resolution. Data acquisition and treatment were carried out with the Wire™ 4.2 software by Renishaw.

#### *Temperature-controlled stage*

For the variable-temperature analysis, the InVia Renishaw Raman spectrometer was coupled with the THMS600/HFS600 temperature-controlled stage (Linkam Scientific Instrument, UK). This is a complete system that provides a stable temperature control that can be programmed from 77 to 873 K. For temperature above 573 K, a water circulation pump must be used to cool the stage. This system allows temperature ramps and holds to be programmed during the required time. The temperature stability is <0.1 K and the sample must be inside the stage between two cover slips 0.2 mm thick to keep the sample in the correct place throughout the experiment. These glass cover slips do not give Raman signal, so they are perfect for this type of work.

### 3.2. Methodology

For this work, all the spectra were collected with the Renishaw microRaman spectrometer and the temperature was programmed with the Linkam THMS600/HFS600 temperature-controlled stage, which was placed inside the spectrometer. To do so, the interlock of the door must be removed.

For the three samples, all the Raman spectra were collected under the same measurement conditions. As the samples did not degrade under high laser powers, the 532 nm excitation diode laser with a 100% of laser power and the 1800 L mm<sup>-1</sup> (vis) grating was used. Each spectrum was acquired with 10 s of exposure time, with the 5× objective and from 100 to 4000 cm<sup>-1</sup>.

The analyses were carried out programming temperature and hold ramps. Each Raman spectra were collected at every -10 K shift from 273 to 83 K. When the desired temperature was reached, it was hold for 6 min. During the hold time, four Raman measurements were performed for checking reproducibility.

After data acquisition, the Raman spectra were treated with the Wire software: the baseline was subtracted from each spectrum and the cosmic rays were removed.

Then, the center, height, full width at half maxim (FWHM) and area of some Raman bands were calculated for several bands of each spectrum. In order to ensure that the experiment was as accurate and precise as possible, the process was systematically repeated for each spectrum.

The curve fitting was also made with the Wire software. This process was carried out by the deconvolution of peaks with a 50% Lorentzian–Gaussian curve. The tolerance used was 0.01 and the width fit of all bands was limited to 100 cm<sup>-1</sup>.

In order to detect outliers, Dixon's Q test was carried out. Then, the parameters versus temperature were plotted, and the linear regression and the Pearson correlation coefficient *r* were calculated. Those plots for which the *r* coefficient was higher than 0.8 were considered as containing a significant trend.

## 4. Results

The Raman spectrum of gypsum is characterized by the bands that appear at 412 (medium, m), 494 (m), 616 (weak, w), 669 (w), 1008 (very strong, vs), 1131 (m), 3405 (s) and 3491 (s)  $\text{cm}^{-1}$  (Prieto-Taboada and others, 2014).

The Raman spectrum of syngenite is characterized by the bands that appear at 132 (very weak, vw), 179 (vw), 200 (vw), 239 (vw), 428 (m), 441 (strong, s), 473 (m), 493 (m), 608 (m), 621 (m), 633 (m), 644 (m) 661 (m), 982 (vs), 1006 (vs), 1083 (vw), 1140 (vw), 1166 (vw) and 3309 (m)  $\text{cm}^{-1}$  (García-Florentino and others, 2021).

The Raman spectrum of görgeyite is characterized by the bands that appear at 429 (w), 439 (w), 475 (w), 480 (m), 604 (w), 631 (m), 661 (w), 980 (s), 1005 (vs), 1012 (vs), 1116 (w), 1138 (w), 1163 (w), 1188 (w), 1216 (vw), 3310 (broad, b), 3412 (b), 3498 (b) and 3527 (b)  $\text{cm}^{-1}$  (García-Florentino and others, 2021).

After doing all the experiments, the values of the temperature-sensitive parameters are shown in Supplementary Tables S1 and S2.

### 4.1 Gypsum

The results obtained from the gypsum study show conclusively that the main and the two water Raman bands exhibit measurable variations in wavenumber when temperature decreases, while the others are apparently unaffected.

In the case of the main gypsum Raman peak ( $\sim 1008 \text{ cm}^{-1}$ ), when the temperature decreased, the band shifted to higher wavenumbers (Table S1, Figs S1, S2). The equation (Eqn (1)) obtained by linear regression for the  $\sim 1008 \text{ cm}^{-1}$  band of gypsum is:

$$\begin{aligned} \text{Band position } (\sim 1008 \text{ cm}^{-1}) &= -0.01277 \cdot T(K) + 1011.88 \\ R^2 &= 0.883 \end{aligned} \quad (1)$$

In the case of the first  $-\text{OH}$  band ( $\sim 3407 \text{ cm}^{-1}$ ), its band position shifted linearly toward higher wavenumbers with decreasing temperature (Table S1, Figs S1, S2). Its equation (Eqn (2)) obtained by linear regression is:

$$\begin{aligned} \text{Band position } (\sim 3407 \text{ cm}^{-1}) &= -0.01621 \cdot T(K) \\ &+ 3410.451 \\ R^2 &= 0.972 \end{aligned} \quad (2)$$

In contrast, the second  $-\text{OH}$  band shifted ( $\sim 3488 \text{ cm}^{-1}$ ) toward lower wavenumber when temperature decreases (Table S1, Figs S1, S2). Its equation (Eqn (3)) obtained by linear regression is:

$$\begin{aligned} \text{Band position } (\sim 3488 \text{ cm}^{-1}) &= 0.0349 \cdot T(K) + 3482.67 \\ R^2 &= 0.943 \end{aligned} \quad (3)$$

However, as can be seen in Table S1, the bandwidth of both  $-\text{OH}$  bands shifted to lower widths when the temperature decreased. In the case of the bandwidth, the distribution of the calibration points is closer to a polynomial function than to a lineal equation. However, the bandwidth is a parameter dependent on several variables apart from the compound itself. In fact, the equipment, optical elements and collection method could affect this band parameter. This, providing linear regressions for bandwidths is not relevant. In any case, it is evident that at low temperature, the  $-\text{OH}$  bands become fairly sharper.

### 4.2 Syngenite

One of the main Raman bands of syngenite ( $\sim 980 \text{ cm}^{-1}$ ) did not undergo significant changes under the temperature changes, in

contrast to its other main band ( $\sim 1006 \text{ cm}^{-1}$ ), which shifted to higher wavenumbers when temperature decreased (Table S2, Figs S1, S2). Its equation (Eqn (4)) obtained by linear regression is:

$$\begin{aligned} \text{Band position } (\sim 1006 \text{ cm}^{-1}) &= -0.02606 \cdot T(K) + 1013.41 \\ R^2 &= 0.955 \end{aligned} \quad (4)$$

Likewise, the two  $-\text{OH}$  bands of syngenite undergo the same band shift, i.e. they shifted toward lower wavenumbers as the temperature decreased (Table S2, Figs S1, S2). However, for the first  $-\text{OH}$  band ( $\sim 3153 \text{ cm}^{-1}$ ), this trend was only observed from 243 to 163 K, so Eqn (5) can only be used between these temperatures. Its equation obtained by linear regression is:

$$\begin{aligned} \text{Band position } (\sim 3153 \text{ cm}^{-1}) &= 0.418 \cdot T(K) + 3039.1 \\ R^2 &= 0.842 \end{aligned} \quad (5)$$

The equation obtained (Eqn (6)) by linear regression for the second  $-\text{OH}$  band ( $\sim 3307 \text{ cm}^{-1}$ ) is:

$$\begin{aligned} \text{Band position } (\sim 3307 \text{ cm}^{-1}) &= 0.0344 \cdot T(K) + 3297.60 \\ R^2 &= 0.934 \end{aligned} \quad (6)$$

The evolution of the syngenite Raman spectra can be seen in Supplementary Figure S2.

### 4.3 Görgeyite

The standard spectrum of görgeyite slightly changes with temperature changes. It could be observed that only one of the main Raman bands ( $\sim 1006 \text{ cm}^{-1}$ ) of görgeyite underwent changes, i.e. the band position of this band shifted to higher wavenumbers when temperature decreased (Table S1, Figs S1, S2). Its equation (Eqn (7)) obtained by linear regression is:

$$\begin{aligned} \text{Band position } (\sim 1006 \text{ cm}^{-1}) &= -0.02180 \cdot T(K) + 1011.99 \\ R^2 &= 0.933 \end{aligned} \quad (7)$$

## 5. Discussion

The changes in the bandwidth and wavenumber shifts are due to the thermal contribution and the changes in the population of the vibrational energy levels (Xie and others, 2001). As can be seen in the trend of the main Raman bands of the three sulfates, these bands exhibit a shift to higher wavenumbers with decreasing temperature. This trend is observed because when temperature decreases, the bonds of the molecules are contracted and, consequently, the strain in the bond increases, causing an increase in energy. Thus, according to Planck's equation (Eqn (8)), when energy ( $E$ ) increases, the frequency ( $\nu$ ) increases and the wavelength ( $\lambda$ ) decreases. Since the wavelength is the inverse of the wavenumber ( $\bar{\nu}$ ), it can be concluded that the increase in energy implies an increase in the wavenumber.

$$E \uparrow = h \cdot \nu \uparrow = h \cdot \frac{c}{\lambda \downarrow} = h \cdot c \cdot \bar{\nu} \uparrow \quad (8)$$

In the case of the Raman  $-\text{OH}$  bands, trends were only observed for gypsum and syngenite. Nevertheless, not the same trend was observed for all these bands, which suggests that each frozen hydration water molecule vibrates depending on the type of ice it forms (Minceva-Sukarova and others, 1984).

Thus, the first –OH band of gypsum followed the same trend as the main bands of the sulfates. In contrast, the second –OH band of gypsum and the two –OH bands of syngenite showed drastic changes upon cooling in the region of the O–H stretch. These bands moved toward lower wavenumbers as temperature decreased. This implies that the indicated O–H bonds are strengthened as temperature decreases (Goncharov, 2012).

Finally, the –OH bands of gypsum were the only ones that underwent changes in the FWHM, as the others did not change sufficiently with temperature to be used as Raman–temperature correlation models. The FWHM of these two bands become narrower as temperature decreases and follow a non-linear rate distribution. This is because the –OH bands become more crystalline and, consequently, were at more ordered energy levels. For that reason, they become narrower and sharper with decreasing temperatures (Cuscó and others, 2016).

As can be seen in Figure S3, the trend obtained in this work is in agreement with Chio and others (2004). On the one hand, the equations of the second hydration band for gypsum are quite similar, being possible to use both. However, the equations of the first hydration band for gypsum differ. Our work possessed a fit of 0.972, while that of Chio and others was 0.886, so the equation proposed in this work is an improved version of that of Chio and others. This difference may be due to, in part, to the extraction methodology used. For example, Chio and others (2004) used a methodology based on a Lorentzian distribution function, whereas in this work 50% Lorentzian–Gaussian curves were used. Likewise, the analyses were limited to a tolerance of 0.01 and the width fit of all bands was limited to 100 cm<sup>-1</sup>.

With the equations estimated in this work, both temperatures and wavenumbers can be calculated for gypsum, syngenite and görgeyite, assuming that one of the two magnitudes is known. Moreover, the uncertainties related to the calibration and the reproducibility of the measurement can be calculated as following:

- (1) Estimate the temperature or Raman wavenumber from Eqns (1)–(7).
- (2) Calculate the uncertainty associated with the measurement, following the equations below. Equation (9) is to calculate the associated uncertainty for temperature ( $\sigma_T$ ) (Miller, 1991) and Eqn (10) for the wavenumber ( $\sigma_{Wn}$ ) (Draper and Smith, 1998).

$$\sigma_x = \frac{S_{x/y}}{m} \sqrt{\frac{1}{p} + \frac{1}{n} + \frac{(\bar{X} - X_0)^2}{\sum (\bar{X} - X_i)^2}} \quad (9)$$

$$\sigma_y = S_{x/y} \sqrt{\frac{1}{p} + \frac{1}{n} + \frac{(\bar{X} - X_0)^2}{S_{xx}}} \quad (10)$$

Being  $S_{U/Wn}$  the standard error of regression,  $m$  the slope of the regression,  $p$  the number of replicates of the sample,  $n$  the points of the calibrate,  $\bar{X}$  the average of the calibration points,  $X_0$  the temperature calculated with the linear regression or the temperature at which the wavenumber is calculated.

- (3) The uncertainty associated with the regression (Eqn (11)) and the reproducibility of the measurement (Eqn (12)) can be calculated.

$$\sigma_{\text{regression}} = \frac{\sigma_{y \text{ or } x}}{\bar{Y} \text{ or } \bar{X}} \quad (11)$$

$$\sigma_{\text{reproducibility}} = \frac{\text{desvest}}{\bar{Y} \text{ or } \bar{X}} \quad (12)$$

- (4) As well as the combined or global uncertainty (Eqn (13)).

$$\text{combined uncertainty} = \sqrt{\sigma_{\text{regression}}^2 + \sigma_{\text{reproducibility}}^2} \quad (13)$$

Two hypothetical examples are given below:

- a) The first hypothetical example would be the estimation of the wavenumber at a certain known temperature: the Martian environmental analyzer of a rover performed four measurements of temperature, being 170.7, 170.5, 171.0 and 169.9 K. Moreover, the instrument equipped with a Raman spectrometer wanted to check if the mineral phase of the analysis point was görgeyite. Thanks to this work, including the Supplementary material data, the wavenumber and the uncertainty of the görgeyite main band can be estimated.
  - a.1) The main band would appear at 1008.276 cm<sup>-1</sup> with a standard derivation of 0.010 cm<sup>-1</sup>, following Eqn (7).
  - a.2) The error associated with the wavenumber ( $Y$ ), following Eqn (10):

$$\sigma_y = 0.35 \sqrt{\frac{1}{4} + \frac{1}{67} + \frac{(170.76 - 170.53)^2}{0.87}} = 34.15$$

- a.3) The uncertainty associated with the regression (Eqn (11)) and with the reproducibility of the measurement (Eqn (12)).

$$\sigma_{\text{regression}} = \frac{34.15}{1008.28} = 3.4 \times 10^{-2}$$

$$\sigma_{\text{reproducibility}} = \frac{0.010}{1008.28} = 1.01 \times 10^{-5}$$

- a.4) The global uncertainty (Eqn (13)).

$$\text{combined uncertainty} = \sqrt{(3.4 \times 10^{-2})^2 + (1.0 \times 10^{-5})^2} = 3.4 \times 10^{-2} \text{ cm}^{-1}$$

Therefore, the wavenumber and the global uncertainty of the görgeyite main band would be 1008.276 ± 0.034 cm<sup>-1</sup>.

- b) The second hypothetical example would be the estimation of the temperature knowing the position of the compound main band: during an in situ measurement campaign in Antarctica, a Raman spectrum of gypsum obtained with the portable Raman spectrometer was obtained. Three measurements of the wavenumber were performed, which appeared at 1008.89, 1008.78 and 1008.87 cm<sup>-1</sup>. However, the scientists were not about the measurement since the instrument did not work well below 123 K. In this sense, thanks to the equations provided, the temperature with its global uncertainty could be calculated.
  - b.1) The Raman wavenumber from Eqn (1). The results would be 237.9 K with a standard derivation of 4.6 K.

b.2) The uncertainty associated with the temperature ( $X$ ), following Eqn (9).

$$\sigma_x = \frac{0.27}{0.013} \sqrt{\frac{1}{3} + \frac{1}{68} + \frac{(169.91 - 237.85)^2}{13889.03}} = 17.52$$

b.3) The uncertainty associated with the regression (Eqn (11)) and the reproducibility of the measurement (Eqn (12)).

$$\sigma_{\text{regression}} = \frac{17.52}{1008.85} = 1.74 \times 10^{-2}$$

$$\sigma_{\text{reproducibility}} = \frac{4.6}{237.85} = 1.93 \times 10^{-2}$$

b.4) The combined uncertainty (Eqn (13)).

$$\begin{aligned} &\text{combined uncertainty} \\ &= \sqrt{(1.74 \times 10^{-2})^2 + (1.93 \times 10^{-2})^2} = 1.8 \times 10^{-2} \text{ K} \end{aligned}$$

Therefore, the temperature and the global uncertainty of the gypsum main band would be  $237.850 \pm 0.012$  K.

## 6. Conclusion

Thanks to this study, it was possible to verify which gypsum, syngenite and görgeyite Raman bands are temperature-sensitive. Likewise, some Raman bands are sensitive to temperature because of two possible effects: (1) they undergo molecular structural changes or (2) temperature causes the distributional change of molecules in various rotational and vibrational energy levels.

In this way, the main bands of the three sulfates shifted toward higher wavenumbers as temperature decreased. The strengthening of the bonds caused an increase in energy and, consequently, higher wavenumbers. However, –OH bands shifted depending on the crystal structure they acquire as the temperature decreased, so not all –OH bands behave in the same way. Finally, the gypsum –OH bands changed to more ordered crystalline structures with decreasing temperature, so their bandwidth decreased.

Based on these trends, it was possible to monitor how temperature-sensitive bands of these sulfates change. Table S3 summarizes the Raman–temperature linear regression equations obtained in this work and the changes that the bands underwent with decreasing temperature.

Thus, it is possible to predict the Raman shift of these compounds down to 83 K. This remarkable regularity of Raman shifts and their temperature dependences, regardless the composition or crystal structure makes it very useful to predict some parameters in cold terrestrial areas such as Antarctica, and in non-terrestrial areas such as the poles of Mars. In addition, this study serves as support science for Mars missions, because the daily temperature ranges from 283 to 193 K and it is continuously measured by dedicated instruments in the current Mars2020 and in the forthcoming MMX and Rosalind Franklin missions.

**Supplementary material.** The supplementary material for this article can be found at <https://doi.org/10.1017/aog.2023.29>.

**Acknowledgements.** J. Huidobro is grateful to the Basque Government predoctoral contract (Ref. PRE\_2022\_2\_0089). J. Aramendia thanks the Basque Government Maria Zambrano contract (Ref. MAZAM21/03).

## References

- Brindley GW and Robinson K (1946) The structure of kaolinite. *Mineralogical Magazine and Journal of the Mineralogical Society* **27**(194), 242–253. doi: [10.1180/minmag.1946.027.194.04](https://doi.org/10.1180/minmag.1946.027.194.04)
- Carter J, Poulet F, Bibring JP, Mangold N and Murchie S (2013) Hydrated minerals on Mars as seen by the CRISM and OMEGA imaging spectrometers: updated global view. *JGR Planets* **118**(4), 831–858. doi: [10.1029/2012JE004145](https://doi.org/10.1029/2012JE004145)
- Chio CH, Sharma SK and Muenow DW (2004) Micro-Raman studies of gypsum in the temperature range between 9 K and 373 K. *American Mineralogist* **89**(2–3), 390–395. doi: [10.2138/am-2004-2-320](https://doi.org/10.2138/am-2004-2-320)
- Chou I-M and Seal RR (2007) Magnesium and calcium sulfate stabilities and the water budget of Mars. *Journal of Geophysical Research* **112**(E11), E11004. doi: [10.1029/2007JE002898](https://doi.org/10.1029/2007JE002898)
- Cloutis EA and 9 others (2007) Stability of hydrated minerals on Mars. *Geophysical Research Letters* **34**(20), L20202. doi: [10.1029/2007GL031267](https://doi.org/10.1029/2007GL031267)
- Couty R, Velde B and Besson JM (1983) Raman spectra of gypsum under pressure. *Physics and Chemistry of Minerals* **10**(2), 89–93. doi: [10.1007/BF00309590](https://doi.org/10.1007/BF00309590)
- Cuscó R, Gil B, Cassabois G and Artús L (2016) Temperature dependence of Raman-active phonons and anharmonic interactions in layered hexagonal BN. *Physical Review B* **94**(15), 155435. doi: [10.1103/PhysRevB.94.155435](https://doi.org/10.1103/PhysRevB.94.155435)
- Draper NR and Smith H (1998) Checking the straight line fit. In Draper N and Smith H (eds), *Applied Regression Analysis*, 3rd Edn. New York: Wiley-Interscience, pp. 47–77. doi: [10.1002/9781118625590.ch2](https://doi.org/10.1002/9781118625590.ch2)
- Ehlmann BL and 6 others (2011) Subsurface water and clay mineral formation during the early history of Mars. *Nature* **479**(7371), 53–60. doi: [10.1038/nature10582](https://doi.org/10.1038/nature10582)
- García-Florentino C and 9 others (2021) Interrelationships in the gypsum–syngenite–görgeyite system and their possible formation on Mars. *Astrobiology* **21**(3), 332–344. doi: [10.1089/ast.2020.2319](https://doi.org/10.1089/ast.2020.2319)
- Gendrin A and 10 others (2005) Sulfates in Martian layered terrains: the OMEGA/Mars express view. *Science* **307**(5715), 1587–1591. doi: [10.1126/science.1109087](https://doi.org/10.1126/science.1109087)
- Goncharov AF (2012) Raman spectroscopy at high pressures. *International Journal of Spectroscopy* **2012**, 1–16. doi: [10.1155/2012/617528](https://doi.org/10.1155/2012/617528)
- Huidobro J, Aramendia J, Arana G and Madariaga JM (2022a) Reviewing in situ analytical techniques used to research Martian geochemistry: from the Viking Project to the MMX future mission. *Analytica Chimica Acta* **1197**, 339499. doi: [10.1016/j.aca.2022.339499](https://doi.org/10.1016/j.aca.2022.339499)
- Huidobro J and 7 others (2022b) Mineralogy of the RBT 04262 Martian meteorite as determined by micro-Raman and micro-X-ray fluorescence spectroscopies. *Journal of Raman Spectroscopy* **53**(3), 450–462. doi: [10.1002/jrs.6291](https://doi.org/10.1002/jrs.6291)
- Madariaga JM and 8 others (2020) Temperature transformation of calcium and potassium Martian sulfates as seen by an Exomars 2022 RLS-like Raman instrument. *14th Europlanet Science Congress 2020*, EPSC2020-1063.
- Miller JN (1991) Basic statistical methods for analytical chemistry. Part 2. Calibration and regression methods. A review. *The Analyst* **116**(1), 3. doi: [10.1039/an9911600003](https://doi.org/10.1039/an9911600003)
- Minceva-Sukarova B, Sherman WF and Wilkinson GR (1984) The Raman spectra of ice (I h, II, III, V, VI and IX) as functions of pressure and temperature. *Journal of Physics C: Solid State Physics* **17**(32), 5833–5850. doi: [10.1088/0022-3719/17/32/017](https://doi.org/10.1088/0022-3719/17/32/017)
- NASA (2023) Mars facts/temperature. Mars Exploration Program website. Available at <https://mars.nasa.gov/all-about-mars/facts/#?c=inspace&s=distance>, (accessed 2023-01-23).
- Nazari-Sharabian M, Aghababaei M, Karakouzián M and Karami M (2020) Water on Mars – a literature review. *Galaxies* **8**(2), 40. doi: [10.3390/galaxies8020040](https://doi.org/10.3390/galaxies8020040)
- Prieto-Taboada N, Laserna O, Martínez-Arkarazo I, Olazabal M and Madariaga J (2014) Raman spectra of the different phases in the CaSO<sub>4</sub>–H<sub>2</sub>O system. *Analytical Chemistry* **86**, 10131–10137. doi: [10.1021/ac501932f](https://doi.org/10.1021/ac501932f)
- Schofield PF, Wilson CC, Knight KS and Stretton IC (2000) Temperature related structural variation of the hydrous components in gypsum. *Zeitschrift Für Kristallographie – Crystalline Materials* **215**(12), 707–710. doi: [10.1524/zkri.2000.215.12.707](https://doi.org/10.1524/zkri.2000.215.12.707)
- Sutherland GBBM (1933) Experiments on the Raman effect at very low temperatures. *Proceedings of the Royal Society of London A: Mathematical and Physical and Engineering Sciences* **141**(845), 535–549. doi: [10.1098/rspa.1933.0137](https://doi.org/10.1098/rspa.1933.0137)

- Szynkiewicz A and Bishop JL** (2021) Assessment of sulfate sources under cold conditions as a geochemical proxy for the origin of sulfates in the circumpolar dunes on Mars. *Minerals* **11**(5), 507. doi: [10.3390/min11050507](https://doi.org/10.3390/min11050507)
- Tuschel D** (2016) Raman thermometry. *Spectroscopy* **31**, 8–13.
- Uddin F** (2008) Clays, nanoclays, and montmorillonite minerals. *Metallurgical and Materials Transactions A* **39**(12), 2804–2814. doi: [10.1007/s11661-008-9603-5](https://doi.org/10.1007/s11661-008-9603-5)
- Weber I and 5 others** (2018) Raman spectra of hydrous minerals investigated under various environmental conditions in preparation for planetary space missions. *Journal of Raman Spectroscopy* **49**(11), 1830–1839. doi: [10.1002/jrs.5463](https://doi.org/10.1002/jrs.5463)
- Xie S, Iglesia E and Bell AT** (2001) Effects of temperature on the Raman spectra and dispersed oxides. *The Journal of Physical Chemistry B* **105**(22), 5144–5152. doi: [10.1021/jp004434s](https://doi.org/10.1021/jp004434s)